

# High-Contrast Object Localization and Removal in Cone-Beam CT

D. J. Moseley,<sup>1</sup> J. H. Siewerdsen<sup>1-3</sup> and D. A. Jaffray<sup>1-4</sup>

<sup>1</sup>Ontario Cancer Institute, Princess Margaret Hospital, Toronto, Ontario, Canada M5G 2M9

<sup>2</sup>Department of Medical Biophysics, University of Toronto, Toronto, Ontario, Canada M5G 2M9

<sup>3</sup>Department of Radiation Oncology, University of Toronto, Toronto, Ontario, Canada M5G 2M9

<sup>4</sup>Radiation Medicine Program, Princess Margaret Hospital, Toronto, Ontario, Canada M5G 2M9

## ABSTRACT

In image-guided procedures, high-contrast objects often appear in the imaging field-of-view for the purpose of guiding treatment (e.g., markers intended to localize the target) or delivering treatment (e.g., surgical tools or in the case of brachytherapy, radioactive seeds). In cone-beam CT reconstructions, these high-contrast objects cause severe streak artifacts, CT number inaccuracy and loss of soft-tissue visibility. We have developed an iterative approach by which high-contrast objects are localized in the 2-D projection set by re-projecting conspicuities from the first-pass 3-D reconstruction. The projection operator, which finds the unique mapping from the world coordinate system to the detector coordinate system for each view angle, is computed from a geometric calibration of the system. In each projection, a two-dimensional 2<sup>nd</sup> order Taylor series is used to interpolate over the high-contrast objects. The interpolated surface is further modified using a local noise estimate to completely mask the high-contrast object. The algorithm has been applied to remove artifacts resulting from a small number of gold fiducial markers in patients being imaged daily with cone-beam CT for guidance of prostate radiotherapy. The algorithm has also been applied to post-operative images of a prostate brachytherapy patient in which the number of seeds can exceed ~100. In each case, the method provides excellent attenuation of image artifact and restoration of soft-tissue visibility. Using a local voxel based metric it was shown that the 2<sup>nd</sup> order Taylor series with added noise performed best at removing the high-contrast objects from the reconstruction volume.

**Key words:** computed tomography, cone-beam CT, image-guided procedures, metal artifacts

## 1. INTRODUCTION

Image-guided procedures often require the placement of high-contrast objects in the field-of-view (FOV). These objects can be used to guide treatment as in the case of fiducial markers<sup>1,2</sup> or deliver treatment as in the case of surgical tools<sup>3</sup> or radioactive brachytherapy seeds.<sup>4</sup> Objects with a high atomic number strongly attenuate x-rays leaving little or no signal in their shadow. This leads to two possible outcomes: 1) photon starvation of the detector or 2) beam hardening of the incident x-ray spectrum. As a result, the reconstructed images suffer from severe streak artifacts,<sup>5</sup> CT number inaccuracy and loss of soft-tissue visibility.

Streak artifacts from high-contrast objects are not unique to cone-beam CT. All slice based CT systems have difficulty with high-contrast objects. A common strategy is to use an interpolative method to replace the missing information in the projection or sinogram space.<sup>5-14</sup> Then the corrected projections can be reconstructed with reduced artifacts. What is unique about the current work is two-fold. Cone-beam CT is a volumetric imaging modality that captures a series of 2-D projection images at multiple view angles. This allows one to interpolate the missing information in two spatial directions. Secondly, since the 2-D information is captured using a quickly pulsed x-ray exposure (5-40ms), all

information is spatially consistent within each projection. Hence, the axial motion of high-contrast objects between frames can be characterized.

Cone-beam CT imaging has been developed on several different platforms to guide therapeutic interventions. The specific platforms discussed in this paper are a medical linear accelerator with a kilo-voltage x-ray source and amorphous silicon flat-panel detector<sup>15</sup> and a mobile isocentric C-arm that allows inter-operative multi-modal fluoroscopy and volumetric imaging.<sup>4</sup>

We propose a method to localize high-contrast objects in cone-beam CT patient images and through a 2-D polynomial interpolation scheme, digitally remove these objects from the projection images. The corrected projections can then be reconstructed without the associated streak artifacts. As a proof of principle, the technique is applied to example patient images from two different cone-beam CT platforms. The two different modalities are the daily setup CT volumes acquired of patients undergoing radiation therapy for prostate cancer and post-operative images of a patient undergoing permanent brachytherapy implant of the prostate using a mobile isocentric C-arm.

The resulting image quality was assessed with several different metrics. Side-by-side comparison of the reconstructed slices allows for a qualitative comparison. For quantitative comparison, difference images of before and after high-contrast object removal show the local and non-local portion of the artifacts that are removed. To analyze the different interpolation schemes, a metric that compared the CT number in the object to the CT number of the surrounding background is computed.

## 2. METHODS AND MATERIALS

### 2.1. Basic Concept

Two basic approaches to high-contrast object removal in CT reconstructions exist. One can either remove the object in the reconstructed image or remove it in each of the projected images before reconstruction. Removing the objects in the reconstructed image is more difficult since the artifacts are non-local. That is, the severe streak artifacts can cover the entire image. For this reason, removal of objects in the projected images (before reconstruction) was pursued. The difficulty with starting with the projection images is that the objects may or may not be obscured by the background anatomy, or could have little contrast to their surroundings in some views. Furthermore, if there are several high-contrast objects in the field of view they may overlap in a projection. Here, the geometric knowledge (e.g. size, shape and orientation) of the high-contrast object acquired from the reconstructions can be used to track the object in each projection. The projected images were first reconstructed using a Feldkamp filtered back-projection method.<sup>16,17</sup> The high-contrast objects are localized in the reconstructions using a histogram-based threshold to yield their 3-D locations in the world coordinate system. The projected pixel location of these objects in each projection can be recovered by using the geometric calibration of the system.<sup>18</sup> Given that the high-contrast objects are localized in the projection space they can be interpolated over using neighbouring pixels that are not contaminated. The interpolation uses a 2<sup>nd</sup> order Taylor series given by

$$\tilde{f} = f(a) + (x - a)^T \cdot \nabla f + (x - a)^T \cdot H(f) \cdot (x - a) + N(\mu, \sigma) + O(\epsilon^3) \quad (1)$$

where  $x \in \mathfrak{R}^2$  is the position of the pixels to be replaced in the 2D image plane and  $a$  is the point about which the interpolation is based (chosen to be the object centroid). The function gradient is denoted by  $\nabla f$ , while  $H(f)$  is the Hessian matrix and  $N(\mu, \sigma)$  is the added noise term. This is a very simple representation. It is low-order and does not require a large number of coefficients to be estimated. The low-order approximation makes the interpolation more robust.

The general concept of the algorithm is illustrated in Fig. 1. Figure 1(a) shows a single 2-D projection image selected from the approximately 320 projection images acquired over 360 degrees. The projection image represents a two-dimensional surface as shown in Fig. 1(b). To remove the high-contrast object, one needs to interpolate this surface. Polynomial interpolations for orders 0, 1 and 2 are shown in Fig. 1(c). Clearly, the 0<sup>th</sup> order interpolation gives the poorest approximation to the surface while the 1<sup>st</sup> and 2<sup>nd</sup> order polynomials fit the profile well.

### 2.1.1. Estimating Polynomial Coefficients

The polynomial coefficients in the 2-D Taylor series of (1) are estimated based on the pixel values on the rim of the high-contrast object. The method to estimate these coefficients depends on the order of the interpolating polynomial used. For example, a 0<sup>th</sup> polynomial is simply a constant. This constant can be estimated by the median value of all pixels on the rim. A 1<sup>st</sup> order polynomial, in addition to the constant term, requires the estimate of the local gradient,  $\nabla f$ . The formula of (1) can be rearranged to yield a linear least-squares problem

$$\begin{bmatrix} (x_1 - a)^T \\ (x_2 - a)^T \\ \vdots \\ (x_n - a)^T \end{bmatrix} \cdot \nabla f = \begin{bmatrix} f(x_1) - f(a) \\ f(x_2) - f(a) \\ \vdots \\ f(x_n) - f(a) \end{bmatrix} \quad (2)$$

where the subscript  $i$  refers to each of the  $n$  points located on the rim of the projected object to be removed. The equation of (2) represents an over-determined system of linear equations and is solved using a QR matrix decomposition. The 2<sup>nd</sup> order polynomial coefficients are more difficult. Since the polynomial contains quadratic terms, the subsequent equation will yield a non-linear least-squares problem given by

$$\min_{\nabla f, H(f)} \left( \sum_{i=1}^n \|f_i - \tilde{f}_i\|^2 \right) \quad (3)$$

where

$$\tilde{f}_i = f(a) + (x_i - a)^T \cdot \nabla f + (x_i - a)^T \cdot H(f) \cdot (x_i - a) \quad (4)$$

are the interpolated rim pixel values and  $f_i$  are the actual rim pixel values. This optimization problem is solved for the polynomial coefficients in (4),  $\nabla f$  and  $H(f)$ , using a Levenberg-Marquardt technique.

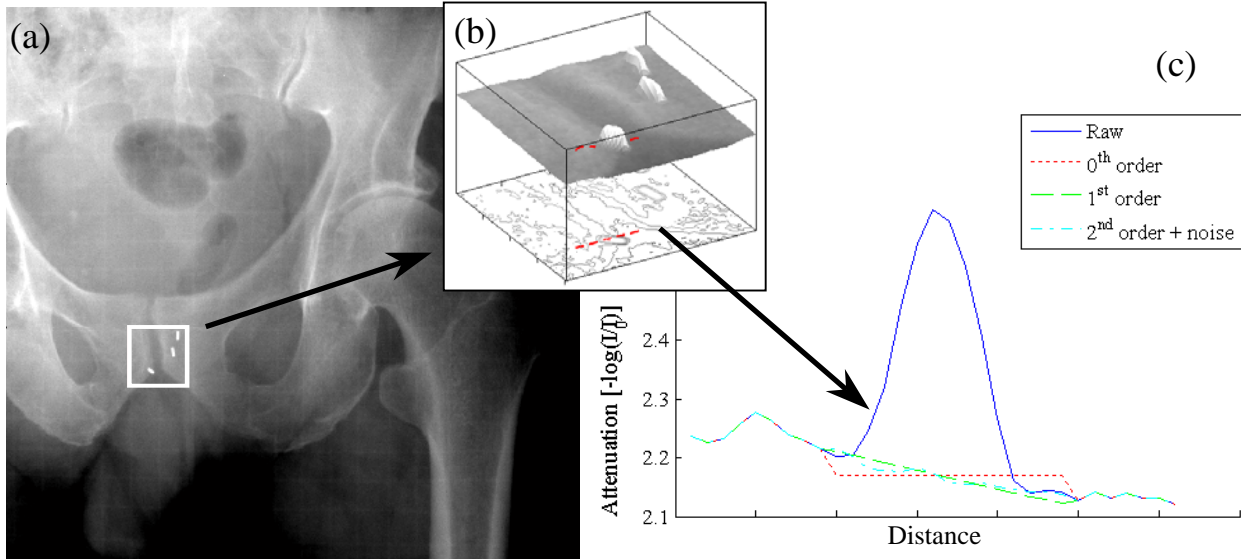


**Figure 1.** Visualization of high-contrast objects in projection images. Here the high-contrast objects are three gold fiducial markers implanted in the prostate of a patient. A 2-D projection image (a) taken during the cone-beam CT acquisition shows the markers. A zoom-in of the small region around the markers yields the surface in (b) where the high-contrast objects are clearly visible. To remove the reconstruction artifacts the 2-D surface must be interpolated in the region of each of the high-contrast objects. A 1-D profile through the marker is shown in (c) where the raw value is interpolated with polynomials of varying order.

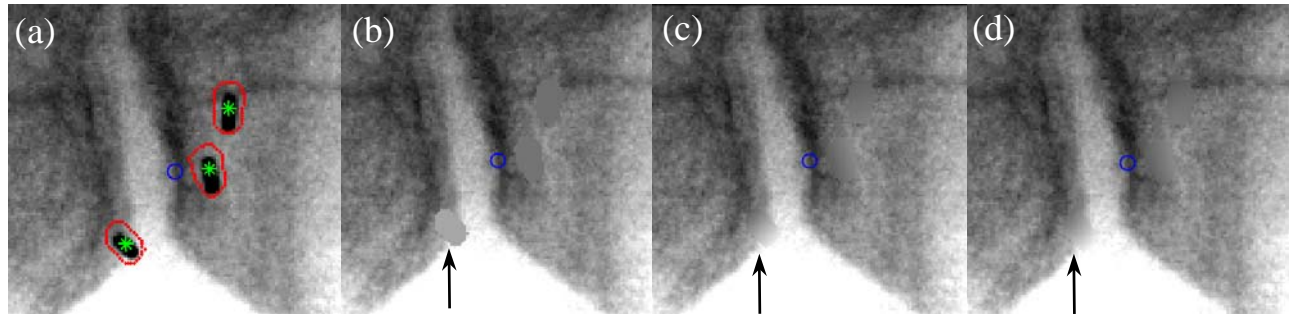


**Figure 2.** (a) Projection image showing 3 high-contrast objects (gold fiducial markers). The seed centers are marked with an asterisk and a dotted line shows the pixels on the rim which will be used to estimate the interpolating polynomial. The objects are replaced with a 2-D polynomial interpolation of (b) 0<sup>th</sup> order, (c) 1<sup>st</sup> order and (d) 2<sup>nd</sup> order. Notice that the seed in the high gradient region (marked with arrow) becomes less visible when using the higher order interpolations.

The interpolation performance as a function of the polynomial order is shown in Fig. 2. The 0<sup>th</sup> order polynomial, constant term, does poorly in areas of high gradient as marked by the black arrow [see Fig. 2(b)]. The interpolation performs better for 1<sup>st</sup> order [see Fig. 2(c)] and 2<sup>nd</sup> order [see Fig. 2(d)]. For the higher order polynomials, the interpolating surface can conform more readily to the projection surface.

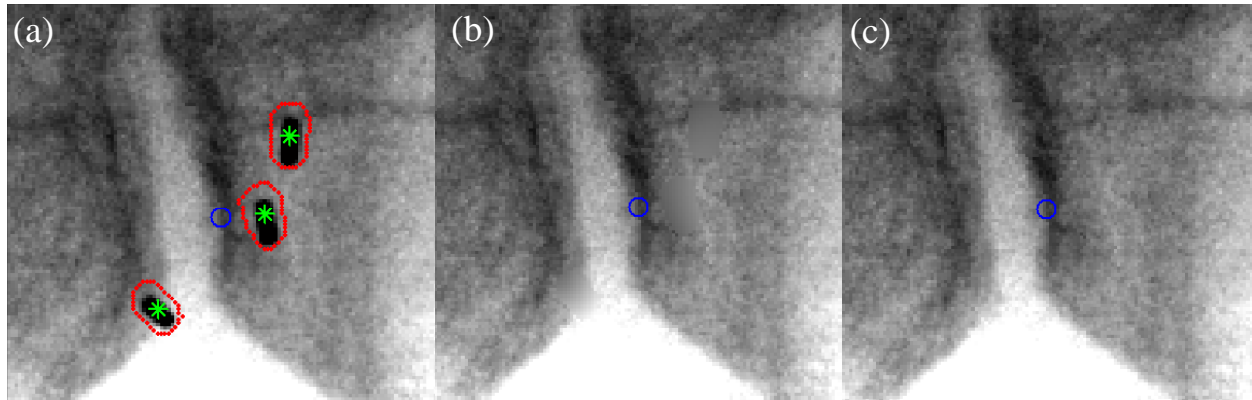


**Figure 3.** (a) Implanted gold fiducial markers in an A-P projection. (b) The high-contrast objects are interpolated over using a 2-D 2<sup>nd</sup> order polynomial. (c) The interpolated regions are further modified by added noise.

### 2.1.2. Added Noise

The 2-D polynomial surface interpolates over the high-contrast object in the projection images but the object is still noticeable since there is an absence of noise in the interpolated region. To overcome this, gaussian noise was added to the interpolated region. The magnitude of the noise was estimated from the pixel values on the rim. The spatial frequency of the added noise was modified by blurring with a kernel estimated from the modulation transfer function (MTF) of the flat-panel detector. Figure 3(a) shows the original image with high-contrast object in place. The asterisk marks the high-contrast object location and the dotted line indicates the rim values which will be used to compute the interpolating polynomial. The second panel [Fig. 3(b)] shows the image interpolated using a 2<sup>nd</sup> order polynomial. Figure 3(c) shows the interpolating surface with added noise. The high-contrast objects are effectively eliminated from the projection image.

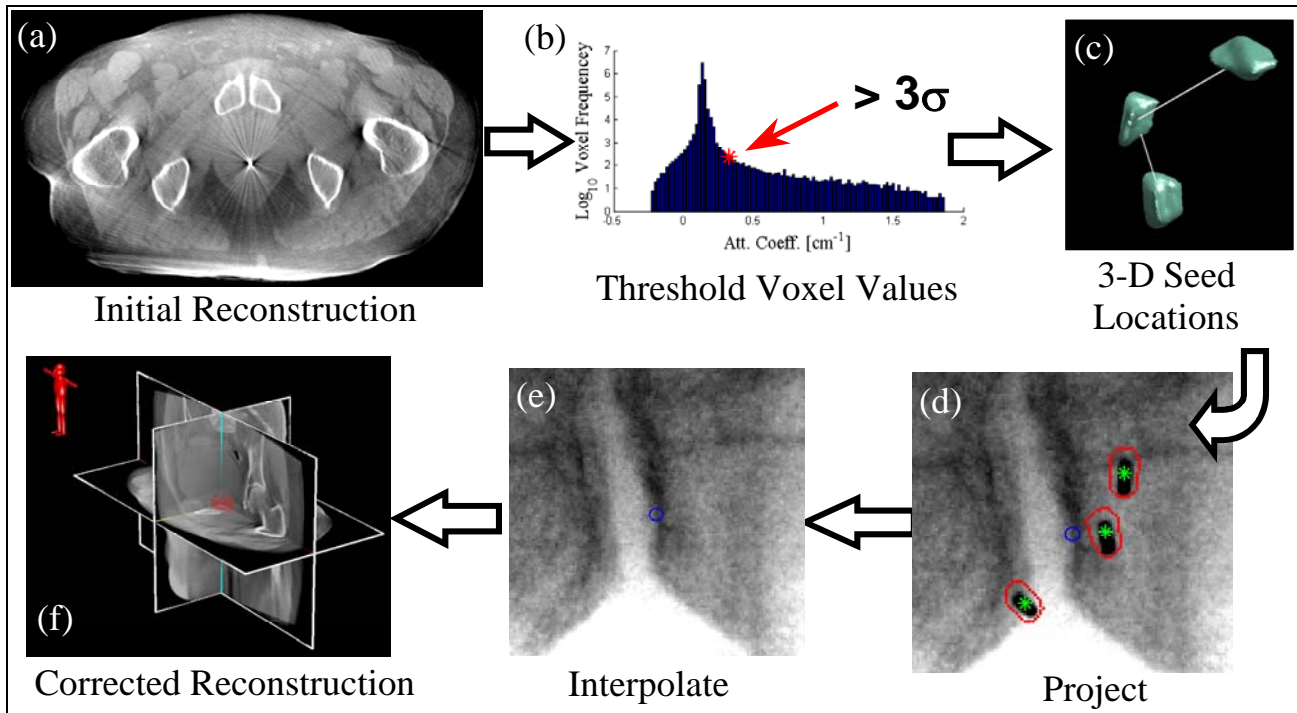


**Figure 4.** Workflow for the removal of high-contrast objects. An initial reconstruction is performed in (a). High-contrast objects are localized based on voxels above a  $3\sigma$  threshold (b) to yield the 3-D position as shown in (c). (d) The location of these voxels and the geometric calibration is used to recover the position of the objects in each of the projection images. (e) The objects are removed by interpolating over the high-contrast regions with a polynomial estimated from the surrounding pixel values. The interpolated images are then sent to the reconstruction algorithm to generate a volumetric image without streaks (f).

## 2.2. Algorithm Workflow

The high-contrast object removal algorithm is applied post-acquisition. The workflow for the algorithm is shown in Fig. 4. An initial reconstruction at a fine voxel pitch [Fig. 4(a)] is performed. The fine pitch allows for more precise localization of the objects to be removed. The high-contrast objects are selected based on voxels lying above a threshold value. The threshold used is the  $3\sigma$  value of the voxel value histogram [Fig. 4(b)]. These voxel locations are further segmented into individual objects [Fig. 4(c)] based on their relative proximity. The 3-D voxel locations for each object are forward projected into the projection image using the geometric calibration. The projected object is dilated by two pixels to account for variation in the projection geometry and seed movement during acquisition. The perimeter (or rim) of uncontaminated pixel values [Fig. 4(d)] estimates the coefficients of the polynomial interpolation given in (2). The interpolated values along with added noise are then used to replace the contaminated projection pixels. This yields a corrected projection [Fig. 4(e)], which is reconstructed into an artifact free volume [Fig. 4(f)].

## 2.3. Geometric Calibration

A key element to this process is to have a precise description of the projection geometry. That is, the mapping between the reconstruction space and the projection space. This will allow the location of objects to be predicted in the projection images based on their position in the world-coordinate system. The imaging geometry for both of the described platforms is not rigid. Flex in the x-ray tube and detector positions change the piercing point of the panel. This mechanical flex has been shown to be reproducible in its behaviour.<sup>15</sup> A geometric calibration is performed using the projection of a single steel ball bearing (BB) positioned at the isocenter of the machine. For the isocentric C-arm, a series of projection matrices are estimated using a spiral pattern of BB's as described in.<sup>19</sup>

### 3. PROSTATE FIDUCIAL MARKERS

#### 3.1. System Description

In our clinic, prostate cancer patients being treated with external beam radiation therapy are imaged daily using a cone-beam CT imaging system that is integrated into the gantry of a medical linear accelerator (Fig. 5a). These patients, however, have fiducial markers implanted in their prostate. The markers, made of 14k gold, are 1mm in diameter and 5 mm long. An 18-gauge needle is used to implant the markers under trans-rectal ultrasound guidance at the apex, base and posterior wall of the prostate. While these seeds are useful for guidance of radiographic imaging modalities, the markers cause significant streak artifacts under CT reconstructions. These streaks cause CT number inaccuracies and obscure soft tissue detail.

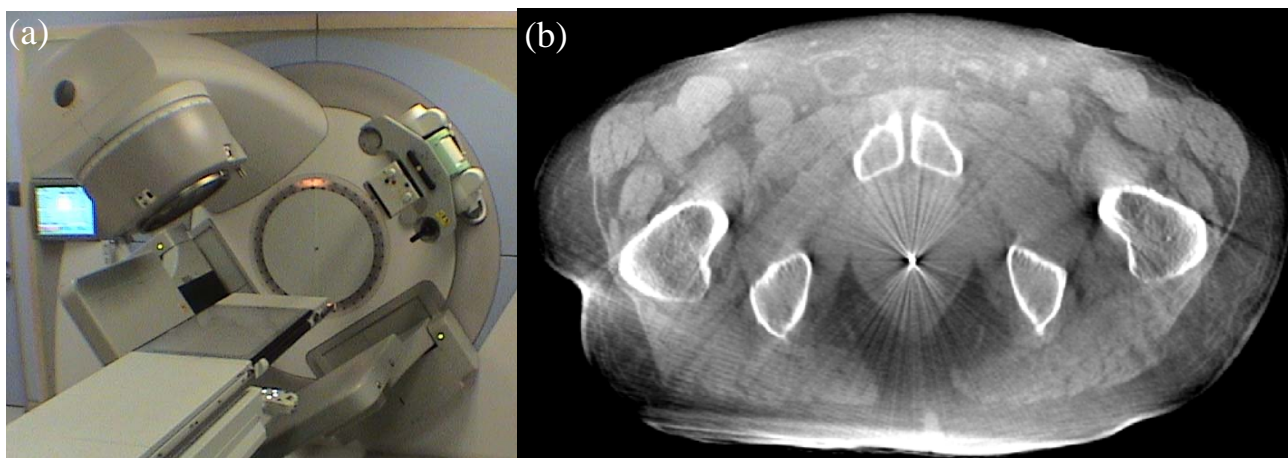


**Figure 5.** (a) Medical linear accelerator with orthogonally mounted x-ray tube and flat-panel detector for acquiring cone-beam CT images of patients undergoing radiotherapy. (b) Streak artifacts in axial slice caused by gold fiducial marker.

#### 3.2. Image Acquisition Details

For cone-beam CT acquisition, the source and detector rotate in a circular trajectory around the patient capturing approximately 320 2-D radiographs through 360°. Each 2-D projection is captured on an amorphous silicon flat-panel detector with  $\text{Gd}_2\text{O}_2\text{S:Tb}$  scintillator. The detector is  $41 \times 41 \text{ cm}^2$  with a  $1024 \times 1024$  image and a pixel pitch of 0.4mm and a 16-bit depth. The imaging geometry consists of a 100cm source-to-axis distance (SAD), and a 153cm source-to-detector distance (SDD), which yields a magnification factor of 1.53. The x-ray technique is 120kVp, 100mA and 20ms yielding an exposure of 2mAs per projection. The estimated patient dose is 2.1cGy to the center of the patient and 3.3 to the periphery (depth 2cm).

#### 3.3. Example Images

Under an ethics approved protocol, 16 prostate patients were scanned before each of their 42 fractions of radiotherapy treatment. The goal of this study was to evaluate the use of soft-tissue targets (as compared to fiducial markers) for the correction of setup errors. To facilitate an unbiased comparison and to reduce image artifacts, the algorithm for marker removal was applied. A total of 315 patient volumes were processed in this manner. For the discussion of results, a single representative patient volume was chosen. The volume is  $40 \times 40 \times 25.6 \text{ cm}$  in extent and reconstructed on a 1mm isotropic voxel grid from 319 projections.

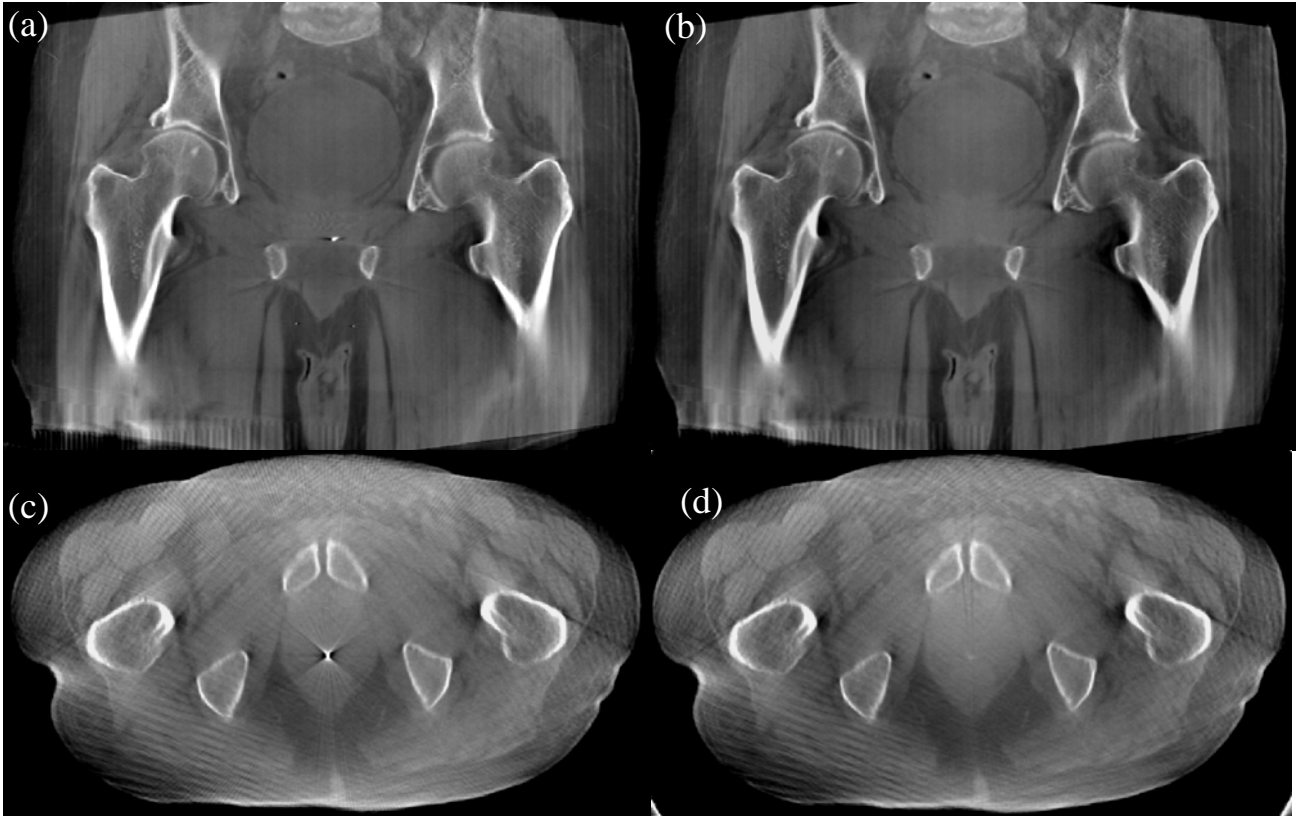


**Figure 6.** Coronal reconstruction slices (a) before and (b) after marker removal. The axial slices are shown in (c) before removal and (d) after removal of the fiducial markers in the projections.

### 3.4. Evaluation of Artifact Removal

Qualitative results for the algorithm are shown in Fig. 6. The reconstruction artifacts associated with the fiducial markers (high CT number and streaks) are eliminated in the final reconstructions [see Fig. 6(b,d)]. It is interesting to note that the other artifacts in the reconstruction remain unchanged. For example, the cupping due to scatter and the beam hardening around the femoral heads is still present. Quantitative analysis of the artifact removal is useful to aid in the choice of algorithm parameters. Two metrics were applied: 1) a difference image of reconstructed slices from before and after fiducial marker removal and 2) the ratio of the fiducial marker voxel values as compared to the background. If the markers are completely erased, the voxel values should be indistinguishable from the background.

#### 3.4.1. Difference Image

A difference image on a single central slice was computed to see the effects of seed removal (see Fig. 7). Figure 7(a) shows the central axial slice of the reconstruction with the fiducial marker and associated streaks present. The markers are completely removed after application of the algorithm as shown in Fig. 7(b). The difference between these two slices, colorwashed in percent, can be seen in Fig. 7(c). The high-contrast objects were removed using a 2<sup>nd</sup> order polynomial with added noise. The corrected reconstruction images show significant difference in the vicinity of the fiducial marker (>100%). The streak artifacts that are removed are on the order of 1% and appear throughout the slice.

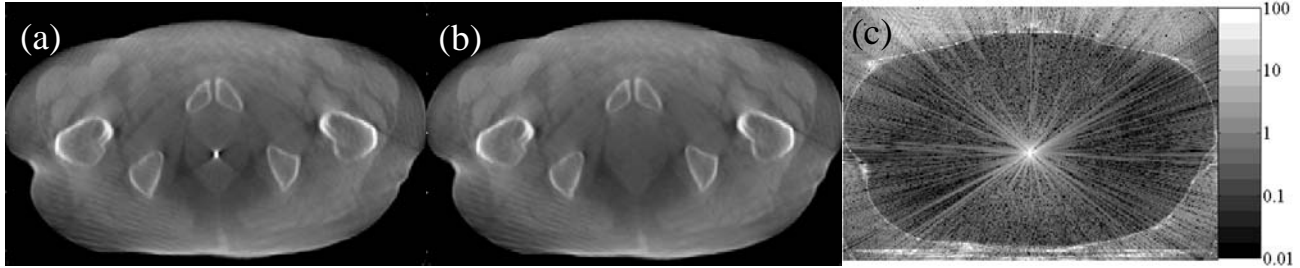


**Figure 7.** Image montage showing percentage differences between (a) central plane axial slice of the original volume and (b) after high-contrast object removal using a 2<sup>nd</sup> order polynomial to interpolate. The difference image (c) is scaled in % based on the color bar. A significant amount of local and non-local artifacts are removed from the processed reconstructions.

**3.4.2. Streak Artifact Remnants**

The effect of high-contrast objects can be separated into local and non-local effects. The local effects include a significant error in CT number estimate on the voxels that contain the high-contrast object as well as shadows around the object caused by beam hardening and detector lag in the wake of the object. The non-local effects include streak artifacts that originate from the edges of the high-contrast region. The streaks are caused by a combination of the ramp-filter enhancing the edges that are back-projected using a finite view-angle sampling density. It is both of these artifacts that we wish to remove/reduce. Figure 8(a) shows two ROI's: one on the high-contrast object (diamonds) and the other a rectangular periphery of voxels that surrounds the object (circles). The ratio of these two regions-of-interest provides a means to see if the object has been removed. By definition, the ratio for the background ROI (circles) is 1 since it will be normalized by itself. The ratio for both ROI's is plotted as a function of interpolation technique. The six interpolation techniques compared are 0<sup>th</sup>, 1<sup>st</sup> and 2<sup>nd</sup> order polynomials with and without added noise. The location of the marker, after removal, should have a CT number similar to that of the background. The ROI that surrounds the high-contrast object will see the streaks passing out from the marker. This will cause higher variability of CT number and be captured in the error bar estimates. Figure 8(b) shows the six techniques on an expanded vertical scale. The CT number of the marker location in the 0<sup>th</sup> order interpolation is nearly 5% higher than the background with very large variability in the voxel values as shown by the errorbars. The 1<sup>st</sup> and 2<sup>nd</sup> order techniques without added noise, however, perform much better. They are 1.2% and 1.1% above background, respectively. With the addition of noise in the interpolation the figures drop even further to 0.8% and 0.7% respectively. Hence, the simple replacement of the high-contrast object with a constant value (0<sup>th</sup> order interpolation) is less effective at removing the streak artifacts. The 1<sup>st</sup> and 2<sup>nd</sup> order interpolations are more effective at removing the markers with a modest increase in performance based on the addition of noise to the interpolated region of the projections.

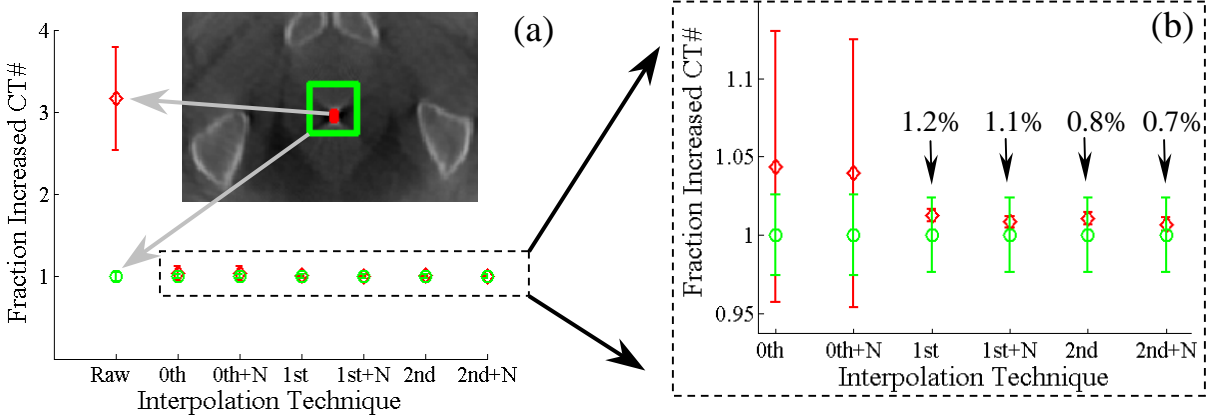


**Figure 8.** (a) Fraction increased CT number shown as a function of the interpolation technique used. The diamond is the average voxel value on the location of the high-contrast object while the circle is based on the line ROI that surrounds the object. (b) An expanded vertical scale which shows the 1<sup>st</sup> and 2<sup>nd</sup> order interpolation are significantly better than the 0<sup>th</sup> order interpolation. The addition of noises helps in reducing the remnants of the high-contrast object.

## 4. BRACHYTHERAPY PERMANENT IMPLANT

The proposed algorithm was applied to the more difficult case of image artifact reduction for a patient receiving permanent implant of brachytherapy seeds. The difficulty arises because of the large number of high-contrast objects involved. A 59-year-old male being treated for Stage I prostate adenocarcinoma was imaged pre-operatively and post-operatively. The brachytherapy implant consisted of 125 Iodine-125 seeds. Each seed, encased in a titanium jacket, is cylindrical in shape and measures 4.5mm in length by 0.8mm in diameter. Normally, the intra-operative procedure requires the patient to be immobilized in the dorsal lithotomy position (legs up). For this post-operative scan, the patient was positioned supine with legs down to make the patient clearance issues less challenging. The images were acquired as a proof-of-principle for the intra-operative procedure.

### 4.1. Image Acquisition

A series of 500 2-D projection images were acquired in 150 seconds over an orbital range of  $180^\circ$  using a Varian 4030CB amorphous silicon flat-panel detector. The flat-panel employs a CsI:TI scintillator over a 2048x1536 photodiode array with pixel pitch of 194  $\mu\text{m}$ . The imaging platform employs the 2x2 binning mode which reads out the panel at 1024x768 pixels of size 388  $\mu\text{m}$  at up to 30 frames per second. The exposure technique was 120kVp, 3.7 mA which resulted in an estimated patient dose of 2.9 cGy. The FOV at isocenter consists of a 20 cm cylinder with 15 cm axial extent.

### 4.2. Seed Localization/Removal

After processing, the projections were reconstructed on a small FOV (10x10x7.5mm) with voxel resolution of 0.2mm. This allowed for precise localization of the seeds including orientation [see Fig. 9(a)]. As before, a voxel value histogram was used to pick a segmentation threshold. Once the seed voxels were acquired, a distance histogram was used to further segment the seed voxels into individual seeds. The seed segmentation was verified using a principal component decomposition. Since the seeds are cylindrical in shape, the largest principal component should correspond to the long axis of the seed. Conversely, the next two singular values correspond to the short axis of the seed. These values should be roughly equal since the seeds are regular in size and cylindrical in shape. The A-P projection selected out of the acquisition set [see Fig. 9(b)] clearly shows the seeds. The interpolation is performed using a 2<sup>nd</sup> order polynomial with added noise to give the corrected images in Fig. 9(c). Now the seed-free projection images can be sent for reconstruction.



**Figure 9** (a) The 3-D locations of the 125 implanted iodine-125 brachytherapy seeds. (b) The A-P projection of the 500 image projection set acquired during scanning showing the implanted seeds. (c) The same projection image but after using a 2<sup>nd</sup> order polynomial to interpolate over each of the seed locations.

## 5. DISCUSSION AND CONCLUSIONS

The proposed technique provides a simple and robust method to reduce reconstruction artifacts caused by high-contrast objects in cone-beam CT images. The novelty of the approach includes the use of the two-dimensional projection information for interpolation through the high-contrast object as well as the addition of noise to the interpolated region. The best performance was achieved with a 2<sup>nd</sup> order polynomial with added noise although this result was only marginally better than a linear interpolation scheme. The method performs well with a small number of small objects (e.g. fiducial markers) as well as a larger number of small objects such as brachytherapy seeds. Extension of the method to larger objects, for example orthopedic implants, will be a challenge and the subject of future investigations.

## ACKNOWLEDGMENTS

The authors gratefully acknowledge the expertise of Steve Ansell, Graham Wilson, and Sami Siddique (Ontario Cancer Institute) on issues of image acquisition and reconstruction. Michel Fresnay from Netherlands Cancer Institute was instrumental in the initial development of the seed knockout concept and Nicholas Tsang (summer student, Michener Institute) did the lion's share of the post-acquisition processing and reconstruction. The cone-beam CT reconstruction algorithm was developed in collaboration with Drs. Rolf Clackdoyle and Frederic Noo (University of Utah). Patient images were acquired by Elizabeth White, M.R.T and Sandra Scott, M.R.T. under protocols headed by Drs C. Catton and J. Crook (Radiation Medicine Program, Princess Margaret Hospital). Support and useful discussions with Dr. Kevin Brown (Elekta Oncology Systems) and the Elekta Synergy Research Group were essential to this work. Dr. Dieter Ritter (Siemens Special Products, Erlangen, Germany) assisted with the acquisition and reconstruction of the C-arm images. This project was supported in part by the National Institutes of Health Grant No. R01-EB002470-04 and R33 AG19381

## REFERENCES

1. H. Alasti, M. P. Petric, C. N. Catton, and P. R. Warde. "Portal imaging for evaluation of daily on-line setup errors and off-line organ motion during conformal irradiation of carcinoma of the prostate," *Int.J.Radiat.Oncol.Biol.Phys.* 49[3]: 869-884 (3-1-2001).
2. S. Aubin, L. Beaulieu, S. Pouliot, J. Pouliot, R. Roy, L. M. Girouard, N. Martel-Brisson, E. Vigneault, and J. Laverdiere. "Robustness and precision of an automatic marker detection algorithm for online prostate daily targeting using a standard V-EPID," *Med.Phys.* 30[7]: 1825-1832 (2003).
3. J. H. Siewerdsen, D. J. Moseley, S. Burch, S. K. Bisland, A. Bogaards, B. C. Wilson, and D. A. Jaffray. "Volume CT with a flat-panel detector on a mobile, isocentric C-arm: Pre-clinical investigation in guidance of minimally invasive surgery," *Medical Physics* 32[1]: 241-254 (2005).
4. J. H. Siewerdsen, D. A. Jaffray, G. K. Edmundson, W. P. Sanders, J. W. Wong, and A. A. Martinez. "Flat-Panel Cone-Beam CT: a Novel Imaging Technology for Image-Guided Procedures," *Mun, Seong K.* 4319[1]: 435-444 (5-28-2001). San Diego, CA, USA, SPIE.
5. W. A. Kalender, R. Hebel, and J. Ebersberger. "Reduction of CT artifacts caused by metallic implants," *Radiology* 164[2]: 576-577 (1987).
6. L. M. Chen, Y. Liang, G. A. Sandison, and J. Rydberg. "Novel Method for Reducing High-Attenuation Object Artifacts in CT Reconstructions," *Sonka, Milan and Fitzpatrick, J. Michael.* 4684[1]: 841-850 (5-15-2002). San Diego, CA, USA, SPIE.
7. G. H. Glover and N. J. Pelc. "An algorithm for the reduction of metal clip artifacts in CT reconstructions," *Med.Phys.* 8[6]: 799-807 (1981).
8. J. Hsieh. "Adaptive streak artifact reduction in computed tomography resulting from excessive x-ray photon noise," *Med.Phys.* 25[11]: 2139-2147 (1998).

9. A. H. Mahnken, R. Raupach, J. E. Wildberger, B. Jung, N. Heussen, T. G. Flohr, R. W. Gunther, and S. Schaller. "A new algorithm for metal artifact reduction in computed tomography: in vitro and in vivo evaluation after total hip replacement," *Invest Radiol.* 38[12]: 769-775 (2003).
10. C. S. Olive, M. R. Kaus, V. Pekar, K. Eck, and L. Spies. "Segmentation-aided adaptive filtering for metal artifact reduction in radio-therapeutic CT images," *Proc.SPIE Int.Soc.Opt.Eng.* 5370[1]: 1991-2002 (5-12-2004).
11. G. Wang, T. Frei, and M. W. Vannier. "Fast iterative algorithm for metal artifact reduction in X-ray CT," *Acad.Radiol.* 7[8]: 607-614 (2000).
12. O. Watzke and W. A. Kalender. "A pragmatic approach to metal artifact reduction in CT: merging of metal artifact reduced images," *Eur.Radiol.* 14[5]: 849-856 (2004).
13. J. Wei, G. A. Sandison, L. Chen, Y. Liang, and L. X. Xu. "X-ray CT high-density artefact suppression in cryosurgery," *Phys.Med.Biol.* 47[24]: N319-N326 (12-21-2002).
14. S. Zhao, D. D. Robertson, G. Wang, B. Whiting, and K. T. Bae. "X-ray CT metal artifact reduction using wavelets: an application for imaging total hip prostheses," *IEEE Trans.Med.Imaging* 19[12]: 1238-1247 (2000).
15. D. A. Jaffray, J. H. Siewerdsen, J. W. Wong, and A. A. Martinez. "Flat-panel cone-beam computed tomography for image-guided radiation therapy," *Int.J.Radiat.Oncol.Biol.Phys.* 53[5]: 1337-1349 (8-1-2002).
16. F. Noo, R. Clackdoyle, C. Mennessier, T. A. White, and T. J. Roney. "Analytic method based on identification of ellipse parameters for scanner calibration in cone-beam tomography," *Phys.Med.Biol.* 45[11]: 3489-3508 (2000).
17. L. A. Feldkamp, L. C. Davis, and J. W. Kress. "Practical cone-beam algorithm," *Journal of the Optical Society of America A: Optics, Image Science, and Vision* 1[6]: 612-619 (1984).
18. Y Cho, D. J. Moseley, J. H. Siewerdsen, and D. A. Jaffray. "Geometric calibration of a cone-beam computed tomography system," *Med.Phys.* in press (2005).
19. R. Fahrig and D. W. Holdsworth. "Three-dimensional computed tomographic reconstruction using a C-arm mounted XRII: image-based correction of gantry motion nonidealities," *Med.Phys.* 27[1]: 30-38 (2000).